Injectorless quantum cascade laser with low voltage defect and improved thermal performance grown by metal-organic chemical-vapor deposition

Dibyendu Dey,[a] Wei Wu, Omer Gokalp Memis, and Hooman Mohseni[b]
Department of Electrical Engineering and Computer Science, Northwestern University, Evanston, Illinois 60208, USA

(Received 6 January 2009; accepted 4 February 2009; published online 24 February 2009)

We demonstrate a strain-compensated injectorless quantum cascade laser (I-QCL), grown by metal-organic chemical-vapor deposition, with a very low voltage defect operating up to room temperature. We experimentally study the effect of voltage defect on thermal performance by comparing the rise in core temperature over a 300 ns pulse width of I-QCL and conventional QCL, working in pulsed mode using time-resolved step scan. I-QCL shows approximately eight times lower rate of rise in core temperature compared to conventional QCL. © *2009 American Institute of Physics*. [DOI: 10.1063/1.3089362]

Quantum cascade laser (QCL) is a unipolar semiconductor light source, which works based on intersubband transition. Since its first demonstration in 1994,[1] rapid developments have been accomplished and already shown room temperature continuous wave operation with high output power in the midinfrared region.[2,3] Recently, much efforts focus on improving its wall-plug efficiency to make it commercially viable in gas and chemical sensing,[4] bioimaging,[5] free space telecommunication,[6] and military applications.[7] Although significant improvements in wall-plug efficiency have been achieved through better active/injector core design, the thermal performance of the laser has not been addressed extensively. In this letter, we address this issue and study the effect of "core design" on voltage defect and thermal performance.

The injectorless QCL (I-QCL) structure presented in this paper works based on a double LO-phonon resonance. The core design is similar to an earlier letter[8] but modified with higher strain ($\sim 3\%$) and doping density. Higher strain increases band offset, which facilitates transfer of electrons and decreases leakage current. The conduction band schematic diagram of two consecutive active regions is shown in Fig. 1. The theoretical predicted switch on electric field is ~ 91 kV/cm and it matches closely with experimentally found result of ~ 88 kV/cm at room temperature.

The epitaxial layer structure was grown by low-pressure metal-organic chemical-vapor deposition. The growth conditions were similar to those reported in an earlier letter[9] with a growth rate for the active region set to be very low (0.1 nm/s) using double-dilution of precursors. The growth was carried out at a temperature of 650 °C at a reactor pressure of 150 Torr using conventional trimethyl reagents, arsine, and phosphine on (100) InP substrate.

The layer sequence of one period is as follows: 6.5/1.0/5.0/1.3/**4.0/2.8/2.8**/1.4/1.2/1.0 nm with bold layers are being doped (Si, 1×10^{17} cm^{-3}) and $In_{0.365}Al_{0.635}As$ barrier layers are printed in italics. All layers were grown on *n*-doped InP substrate (2.0×10^{17} cm^{-3}). The injectorless structure has 60 active regions sandwiched between two 500 nm *n*-doped $In_{0.53}Ga_{0.47}As$ (Si, 5.0×10^{16} cm^{-3}) layers. The upper cladding consists of a 2.5 μm *n*-InP (Si, 1.0×10^{17} cm^{-3}), followed by 800 nm n^+-$In_{0.53}Ga_{0.47}As$ (Si, 5.0×10^{18} cm^{-3}) and 200 nm thick n^+-$In_{0.53}Ga_{0.47}As$ (Si, 3.0×10^{19} cm^{-3}).

After in-depth growth condition optimization, good material quality was demonstrated from epitaxial characterizations. The appearance of numerous sharp and narrow satellite peaks indicates the excellent interface quality and growth uniformity as shown in Fig. 2. The closeness of simulated and experimental data indicates an excellent uniformity and control over layer thickness, material composition, and interface switching across the entire 60 period layer structure.

The growth structure was defined into double trench ridges using standard photolithography with varying ridge widths ranging from 10 to 25 μm. A second photolithographic mask formed an opening pattern on the top of the ridge and it was used as the mask to dry etch plasma-enhanced chemical-vapor deposition deposited 300 nm Si_3N_4. The top contact was formed with Ti/Pt/Au (20/50/500 nm). The wafer was thinned to 100 μm and the back contact was formed with Ge/Au/Ni/Au (12/25/50/500 nm). Contacts were annealed with rapid thermal annealing at 380 C for 1 min.

The output power and applied voltage versus current (*L-I-V*) characteristic was obtained with the mounted device

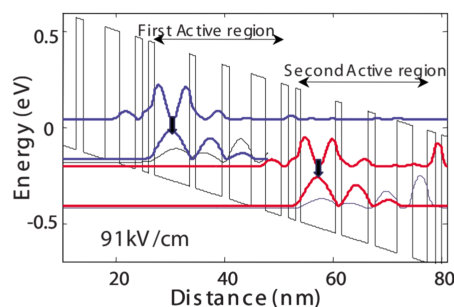

FIG. 1. (Color online) Conduction band diagram of $In_{0.365}Al_{0.635}As/In_{0.65}Ga_{0.35}As$ I-QCL under a positive bias corresponding to an applied voltage of 91 kV/cm. Two successive active regions are shown and the black thick arrow indicates the lasing transition at 184 meV.

[a]Electronic mail: dey@u.northwestern.edu.
[b]Electronic mail: hmohseni@ece.northwestern.edu.

 © 2009 American Institute of Physics

Downloaded 24 Feb 2009 to 165.124.162.126. Redistribution subject to AIP license or copyright; see http://apl.aip.org/apl/copyright.jsp

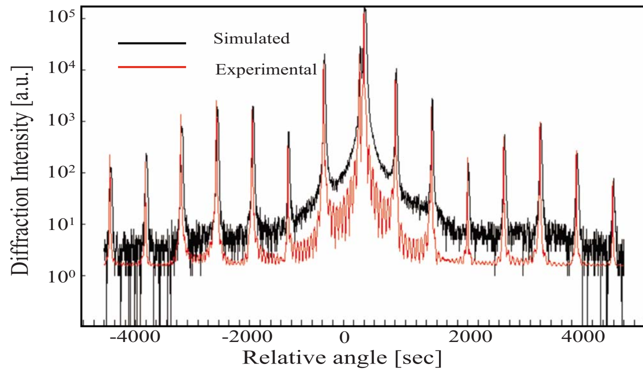

FIG. 2. (Color online) Experimental and simulated x-ray diffraction curve of a 60-period strain-compensated I-QCL structure.

placed on a temperature-controlled cold finger of a nitrogen-cooled cryostat and the detector was a liquid nitrogen cooled fast HgCdTe detector with a ~15 ns rise and fall time. All measurements were performed in pulsed mode operation with a pulse width of 300 ns and a repetition frequency of 1 kHz. The measured device dimensions were 2.1 mm $\times 30$ μm. Figure 3 shows the pulsed light output-current characteristics of the injectorless device at different heat sink temperatures as well as the voltage-current plot at room temperature. The threshold voltage was found to be ~14.1 V at 77 K and ~14.4 V at 250 K. Threshold current density (J_{th}) and sink temperature (T) were fit using an exponential function: $J_{th}=J_0 \exp(T/T_0)$ and it gave a characteristic temperature (T_0) of 125 K. Using the threshold voltage and assuming that the entire voltage drop occurs over an active core (voltage defect overestimation), a voltage defect of 57 meV was calculated at 77 K and 67 meV at 250 K. A conventional QCL "with injector," similar to a design described in Ref. 10, was also measured with the same measurement setup. The device had the same dimension as I-QCL and was fabricated by similar two steps standard photolithography process described earlier. Voltage defect of 120 meV at 77 K was measured for this device with a lasing wavelength of 4.8 μm.

Voltage defect represents the electrical power, which does not contribute to the optical power output of the laser. Presence of injectors in conventional QCL help transferring electrons from one active region to the next but at the cost of generating more heat due to additional phonon relaxation

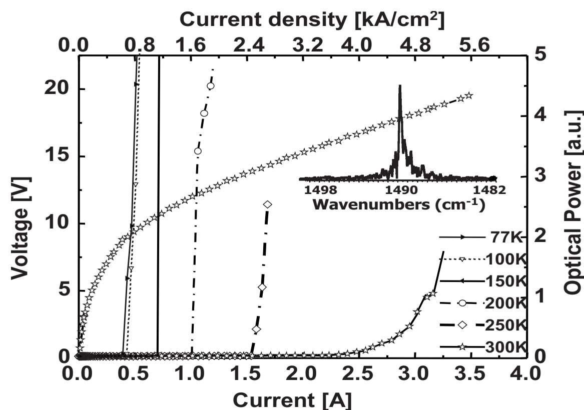

FIG. 3. Pulsed light output power-current (L-I) characteristics of a 2.1 mm long and 25 μm wide episide up I-QCL device in the 77–300 K range. The current voltage curve (I-V) at 300 K is plotted together. The inset shows emission spectrum at 77 K where lasing peak wavelength is 1488 cm^{-1}.

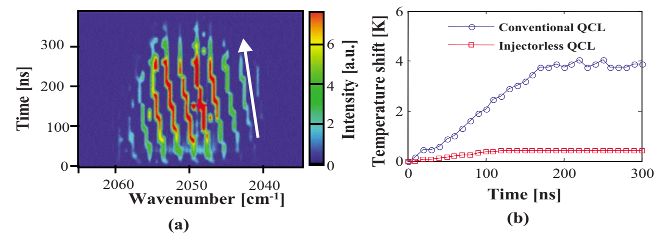

FIG. 4. (Color online) (a) Time-resolved step scan picture showing thermal shift in wavelength due to rise in core temperature for QCL with injector. The inserted white arrow indicates the direction of shift in lasing wavelength. (b) Comparison of the rise in core temperature of conventional QCL and I-QCL at room temperature.

inside the injectors. I-QCL design, presented in this paper, directly transfers electrons from one active region to the next one. Such design reduces the heat generation due to the absence of any injectors where additional phonon relaxation takes place. Thus "wasted heat" in the core gets reduced and "voltage defect" is expected to be lower. For comparison, recently shown heterogeneous injector design has a voltage defect of 79 meV (Ref. 11) and conventional QCL has a voltage defect of 140 meV (Ref. 12) at 77 K, which is higher compared to voltage defect reported here.

In order to study the effect of the reduced number of phonons generated per cascade layer, we measured the instantaneous core temperature of the laser working in pulsed mode. In principle, generation of heat in the laser core shifts the lasing wavelength to lower energies (longer wavelength) and can be measured using time resolved step scans. Rise in core temperature of the lasers is related with thermal shift in lasing wavelength with the following formula:[13]

$$\Delta T = \frac{\Delta k}{k}\left(\alpha + \frac{\beta}{n_{eff}}\right)^{-1}, \tag{1}$$

where n_{eff} represents effective refractive index of core material and represent linear thermal expansion coefficient of the semiconductor and temperature coefficient of change in refractive index, respectively, k is the wave number and Δk is change in wave number.

The shift in core temperature over a pulse width of 300 ns was estimated using Eq. (1) where thermal shift in lasing modes was measured using time-resolved step scan with Nicholet 8700 Fourier transform infrared spectrometer. The time and frequency resolution were 10 ns and 0.125 cm^{-1}, respectively. We used the linear thermal expansion coefficient (α) of 5.66×10^{-6} K^{-1} for $In_{0.65}Ga_{0.35}As$ and 5.4×10^{-6} K^{-1} for $In_{0.365}Al_{0.635}As$.[14] The temperature coefficient of change in refractive index (β) for $In_{0.65}Ga_{0.35}As$ and $In_{0.365}Al_{0.635}As$ were estimated to be 7.8×10^{-4} [15,16] and 3.5×10^{-4} K^{-1},[17] respectively. Change in refractive index due to variation in carrier concentration was neglected since the current was uniform over the pulse width and "carrier clamping" happens above threshold voltage. The rise in core temperature of QCL and I-QCL are plotted together in Fig. 4(b). The lasing wavelength starts to shift with time at the beginning, which indicates a near monotonic core temperature increase, as seen from the slope of the curve in Fig. 4(b). Temperature rise gets saturated as a thermal equilibrium is reached overtime. Conventional QCL shows a rate of change

Downloaded 24 Feb 2009 to 165.124.162.126. Redistribution subject to AIP license or copyright; see http://apl.aip.org/apl/copyright.jsp

in core temperature 1.3×10^{7} K/s, approximately eight times faster compared to I-QCL.

In summary, we have demonstrated an I-QCL that has low voltage defect of 57 meV at 77 K at an emission wavelength of 6.7 μm. This value is smaller than previously reported "voltage defects" of other QCLs. We believe that the lower number of "phonon relaxations" inside the injectorless design compared to conventional design, is the source of this reduced voltage defect. Working in pulsed mode at 77 K, we experimentally found that the rise of laser core temperature was approximately eight times higher for conventional QCL compared to I-QCL. This is bigger than the expected as conventional QCL design has four-phonon emission compared to two-phonon emission in case of I-QCL per laser stage. It is not clear why a factor of 2 reduction in phonon emission per stage can produce an almost eight times reduction in temperature rise in I-QCL. We attribute this anomaly to nonlinear thermal behavior of QCL that is observed and described in detail by others.[18,19] These effects include thermal backfilling of lower laser level, temperature dependent thermal conductivity, thermionic excitation of carriers, and phonon assisted carrier lifetime. As the core temperature rises during a pulse, the process of thermally activated backfilling increases rapidly and more LO phonons get generated. This could reduce injection efficiency and increases free carrier absorption, resulting in increased heat generation. Further, thermionic emission current is reintroduced into the cascade and additional phonons are generated in conventional QCL. All other processes also have a strong nonlinear dependence on core temperature.

In conclusion, we measured the evolution of core temperature of QCL in pulsed mode. The I-QCL demonstrated here has improved thermal performance compared to conventional QCL due to its favorable core design.

This work is partly supported by Defense Advanced Research Agency (DARPA), under Grant No. N00014-07-1-0564.

[1] J. Faist, F. Capasso, D. L. Sivco, C. Sirtori, A. L. Hutchinson, and A. Y. Cho, Science **264**, 553 (1994).
[2] A. Lyakh, C. Pflugl, L. Diehl, Q. J. Wang, F. Capasso, X. J. Wang, J. Y. Fan, T. Tanbun-Ek, R. Maulini, A. Tsekoun, R. Gao, and C. K. N. Patel, Appl. Phys. Lett. **92**, 111110 (2008).
[3] Y. Bai, S. R. Darvish, S. Slivken, W. Zhang, A. Evans, J. Nguyen, and M. Razeghi, Appl. Phys. Lett. **92**, 1011051 (2008).
[4] J. P. Lima, H. Vargas, A. Miklos, M. Angelmahr, and P. Hess, Appl. Phys. B: Lasers Opt. **85**, 279 (2006).
[5] A. A. Kosterev, F. K. Tittel, W. Durante, M. Allen, R. Kohler, C. Gmachl, F. Capasso, D. L. Sivco, and A. Y. Cho, Appl. Phys. B: Lasers Opt. **95**, 74 (2002).
[6] J. Faist, Opt. Photonics News **17**, 32 (2006).
[7] A. W. M. Lee and Q. Hu, Opt. Lett. **30**, 2563 (2005).
[8] S. Katz, A. Friedrich, G. Boehm, and M. C. Amann, Appl. Phys. Lett. **92**, 181103 (2008).
[9] M. Troccoli, D. Bour, S. Corzine, G. Hofler, A. Tandon, D. Mars, D. J. Smith, L. Diehl, and F. Capasso, Appl. Phys. Lett. **85**, 5842 (2004).
[10] A. Evans, J. S. Yu, S. Slivken, and M. Razeghi, Appl. Phys. Lett. **85**, 2166 (2004).
[11] A.J.Hoffman, S. Schartner, S.Howard, K. J. Franz, F. Towner, and C. Gmachl, Opt. Express **15**, 15818 (2007).
[12] A. Evans, S. R. Darvish, S. Slivken, J. Nguyen, Y. Bai, and M. Razeghi, Appl. Phys. Lett. **91**, 071101 (2007).
[13] J. T. Verdeyen, *Laser Electronics*, 3rd ed. (Prentice-Hall, Englewood Cliffs, NJ, 1994).
[14] M. Levinstein, S. Rumyantsev, and M. Shur, *Handbook Series on Semiconductor Parameters* (World Scientific, Singapore, 1996), Vols. 1–2.
[15] J. Piprek, H. Wenzel, and G. Sztefka, IEEE Photonics Technol. Lett. **6**, 139 (1994).
[16] H. C. Casey and M. B. Panish, *Heterostructure Lasers, Part A* (Academic, New York, 1978).
[17] B. Jensen and W. D. Jensen, IEEE J. Quantum Electron. **27**, 40 (1991).
[18] S. S. Howard, Z. Liu, D. Wassermann, A. J. Hoffman, T. S. Ko, and C. F. Gmachl, IEEE J. Sel. Top. Quantum Electron. **13**, 1054 (2007).
[19] S. S. Howard, Z. Liu, and C. F. Gmachl, IEEE J. Quantum Electron. **44**, 319 (2008).

Downloaded 24 Feb 2009 to 165.124.162.126. Redistribution subject to AIP license or copyright; see http://apl.aip.org/apl/copyright.jsp